3-2001

The N-terminal Segment of Recombinant Porcine Fructose-1,6-bisphosphatase Participates in the Allosteric Regulation of Catalysis

Scott W. Nelson
Iowa State University, swn@iastate.edu

Feruz T. Kurbanov
Iowa State University

Richard B. Honzatko
Iowa State University, honzatko@iastate.edu

Herbert J. Fromm
Iowa State University

The N-terminal Segment of Recombinant Porcine Fructose-1,6-bisphosphatase Participates in the Allosteric Regulation of Catalysis

Abstract

Residues 1–10 of porcine fructose-1,6-bisphosphatase (FBPase) are poorly ordered or are in different conformations, sensitive to the state of ligation of the enzyme. Deletion of the first 10 residues of FBPase reducesk_{cat} by 30-fold and Mg^{2+} affinity by 20-fold and eliminates cooperativity in Mg^{2+} activation. Although a fluorescent analogue of AMP binds with high affinity to the truncated enzyme, AMP itself potently inhibits only 50% of the enzyme activity. Additional inhibition occurs only when the concentration of AMP exceeds 10 mM. Deletion of the first seven residues reduces k_{cat} and Mg^{2+} affinity significantly but has no effect on AMP inhibition. The mutation of Asp^{9} to alanine reproduces the weakened affinity for Mg^{2+} observed in the deletion mutants, and the mutation of Ile^{10} to aspartate reproduces the AMP inhibition of the 10-residue deletion mutant. Changes in the relative stability of the known conformational states for loop 52–72, in response to changes in the quaternary structure of FBPase, can account for the phenomena above. Some aspects of the proposed model may be relevant to all forms of FBPase, including the thioredoxin-regulated FBPase from the chloroplast.

Keywords

Biocatalysts, Enzyme inhibition, Magnesium printing plates, fructose bisphosphatase, isoleucine, thioredoxin, enzyme kinetics

THE JOURNAL OF BIOLOGICAL CHEMISTRY
Vol. 276, No. 9, Issue of March 2, pp. 6119–6124, 2001

Printed in U.S.A.

The N-terminal Segment of Recombinant Porcine Fructose-1,6-bisphosphatase Participates in the Allosteric Regulation of Catalysis*

Received for publication, October 17, 2000
Published, JBC Papers in Press, November 28, 2000, DOI 10.1074/jbc.M009485200

Scott W. Nelson, Feruz T. Kurbanov‡, Richard B. Honzatko, and Herbert J. Fromm§

From the Department of Biochemistry, Biophysics, and Molecular Biology, Iowa State University, Ames, Iowa 50011

Residues 1–10 of porcine fructose-1,6-bisphosphatase (FBPase) are poorly ordered or are in different conformations, sensitive to the state of ligation of the enzyme. Deletion of the first 10 residues of FBPase reduces k_{cat} by 30-fold and Mg^{2+} affinity by 20-fold and eliminates cooperativity in Mg^{2+} activation. Although a fluorescent analogue of AMP binds with high affinity to the truncated enzyme, AMP itself potently inhibits only 50% of the enzyme activity. Additional inhibition occurs only when the concentration of AMP exceeds 10 mM. Deletion of the first seven residues reduces k_{cat} and Mg^{2+} affinity significantly but has no effect on AMP inhibition. The mutation of Asp^{9} to alanine reproduces the weakened affinity for Mg^{2+} observed in the deletion mutants, and the mutation of Ile^{10} to aspartate reproduces the AMP inhibition of the 10-residue deletion mutant. Changes in the relative stability of the known conformational states for loop 52–72, in response to changes in the quaternary structure of FBPase, can account for the phenomena above. Some aspects of the proposed model may be relevant to all forms of FBPase, including the thioredoxin-regulated FBPase from the chloroplast.

Fructose-1,6-bisphosphatase (D-fructose 1,6-bisphosphate 1-phosphohydrolase, EC 3.1.3.11; FBPase[1]) catalyzes the hydrolysis of fructose 1,6-bisphosphate ($F16P_2$) to fructose 6-phosphate and inorganic phosphate (P_i) (1–3). The reaction facilitated by FBPase is subject to hormone and metabolite regulation, the net result of which is the tight coordination of FBPase and fructose 6-phosphate 1-kinase activities (4). FBPase activity requires divalent cations such as Mg^{2+}, Mn^{2+}, or Zn^{2+}, and plots of velocity *versus* metal ion concentration are sigmoidal with a Hill coefficient of 2.0 (5–7). AMP binds cooperatively (Hill coefficient of 2) 28 Å from the nearest active site (8) and inhibits the enzyme, whereas $F26P_2$ binds at the active site (9). Inhibition of FBPase by AMP and $F26P_2$ is synergistic. $F26P_2$ can lower the apparent inhibition constant for AMP by up to 10-fold (6).

FBPase is a tetramer of identical subunits (M_r = 37,000). To a first approximation, these subunits lie in the same plane and occupy the corners of a square in one of the principal quaternary states of the mammalian enzyme (R-state). By past convention, subunit C1 occupies the upper left-hand corner, with subunits C2–C4 following in a clockwise direction. AMP causes a transition from the R-state to the T-state, driving a 17° rotation of the C1-C2 subunit pair with respect to the C3-C4 pair about a molecular 2-fold axis of symmetry (10). Complexes of FBPase with AMP in the presence of $F16P_2$, $F26P_2$, and fructose 6-phosphate are all in the T-state (9, 11, 12), whereas in the absence of AMP, the enzyme has appeared in the R-state in crystal structures (13, 14).

Mutations in loop 52–72 and in the hinge preceding the loop (residues 50–51) greatly influence catalysis and AMP inhibition of FBPase and together suggest the necessity of an engaged conformation for loop 52–72 for catalysis under physiological conditions (15, 16). The engaged conformation, in which loop 52–72 interacts with the active site, occurs in metal-product complexes of wild-type FBPase but only in the absence of AMP (17). All residues of the engaged loop are in well defined conformations associated with clear electron density in crystal structures (13, 14). The disengaged conformation of loop 52–72 exists in AMP complexes of wild-type FBPase. The disengaged loop is far from the active site. Residues 52–60 lie near, and interact with, an adjacent subunit (C1-C2 interaction), but residues 61–73 are disordered, with no observable electron density in crystal structures (14). In FBPase crystallized without metal cations (18) and in certain mutant forms of FBPase (to be discussed below in greater detail), loop 52–72 exists in yet another conformation in which residues 54–73 are without electron density. This disordered state of the loop 52–72 is a manifold of closely related conformations in which the loop itself interacts weakly with the rest of the enzyme.

AMP binds between helices H1 and H2 of FBPase and causes modest movements in both helices relative to the rest of the subunit (14). The 0.9-Å movement of helix H2 along its axis directly influences loop 52–72 (13), whereas the 1.5-Å movement of helix H1 could influence loop 52–72 of an adjacent subunit (14). AMP may stabilize the disengaged conformation of loop 52–72 through helix H1 by facilitating contacts between residues 52–59 of the loop and residues 1–10 of the N terminus. Residues belonging to this N-terminal segment are either disordered (residues 1–6) or exist in different conformations in the R- and T-state of FBPase (residues 7–10). In addition, several of these N-terminal residues are conserved throughout FBPases from eukaryotes, suggesting a functional significance, as yet unconfirmed.

Here we present the changes in functional properties of

* This work was supported in part by National Institutes of Health Research Grant NS 10546 and National Science Foundation Grants MCB-9603595 and MCB-9316244. This is Journal Paper 19128 of the Iowa Agriculture and Home Economic Experiment Station, Ames, Project 3191. The costs of publication of this article were defrayed in part by the payment of page charges. This article must therefore be hereby marked "*advertisement*" in accordance with 18 U.S.C. Section 1734 solely to indicate this fact.

‡Present address: Dept. of Molecular and Cell Biology, University of California, Berkeley, California 94720.

§ To whom correspondence should be addressed. Tel.: 515-294-4971; Fax: 515-294-0453; E-mail: hjfromm@iastate.edu.

[1] The abbreviations used are: FBPase, fructose-1,6-bisphosphatase; $F16P_2$, fructose 1,6-bisphosphate; $F26P_2$, fructose 2,6-bisphospate; P_i, orthophosphate; CD, circular dichroism; AMP-PNP, 2′-(or 3′)-*O*-(trinitrophenyl) adenosine 5′-monophosphate.

FBPase due to deletion and point mutations in the N-terminal segment (residues 1–10). Mutations, which directly or indirectly influence positions 9 and 10, cause large perturbations in catalysis and/or AMP inhibition. A simple model in which the quaternary states of FBPase differentially stabilize specific conformations of loop 52–72 accounts for the properties of wild-type and mutant FBPases presented here and in other studies.

EXPERIMENTAL PROCEDURES

Materials—$F16P_2$, $F26P_2$, $NADP^+$, and AMP were purchased from Sigma. DNA-modifying and restriction enzymes, T4 polynucleotide kinase, and ligase were from Promega. Glucose-6-phophate dehydrogenase and phosphoglucose isomerase came from Roche Molecular Biochemicals. Other chemicals were of reagent grade or equivalent. *Escherichia coli* strains BMH 71–18 mutS and XL1-Blue came from CLONTECH and Stratagene, respectively. The FBPase-deficient *E. coli* strain DF 657 came from the Genetic Stock Center at Yale University.

Mutagenesis of Wild-type FBPase—Mutations were accomplished by deletion of or specific base changes in double-stranded plasmid using the Transformer™ site-directed mutagenesis kit (CLONTECH). The mutagenic primers are as follows: 10DEL, 5′-GAAGGAGATATACAT-**ATGGTC**ACCCTAACCCGCTTCGTCATGGAG-3′; 7DEL, 5′-GTTTAA-CTTTAAGAAGGAGATATACATA**ATGACC**AATATCGTCACCCTAA-CCCGCCTCG-3′; $Ile^{10} \rightarrow$ Asp, 5′-ACACCAAT**GAC**GTCACCC-3′; $Ile^{10} \rightarrow$ Met 5′-ACACCAAT**ATG**GTCACCC-3′; $Asn^9 \rightarrow$ Ala, 5′-CCTTCGAC-ACC**GCT**ATCGTCACCC-3′; $Thr^8 \rightarrow$ Ala, 5′GGCCTTCGAC**GCC**AAT-ATCGTC-3′; $Asp^7 \rightarrow$ Ala, 5′CGGCCTTC**GCC**ACCAATATCGTC-3′; $Phe^6 \rightarrow$Trp, 5′-GACCAGGCGGCC**TGG**GACACCATTATC-3′; and $Asp^2 \rightarrow$ Ala, 5′-ACATATGACG**GCC**CAGGCGGC3′ (codons spanning deletions and codons for point mutations are underlined in bold typeface). The selection primer for mutagensis, which changed an original *Nru*I site on the plasmid into a *Xho*I site was 5′-CAGCCTCGC**CTCGAG**A-ACGCCA-3′ (digestion site underlined in bold typeface). The mutations and integrity of the constructs were confirmed by sequencing the promoter region and the entire open reading frame. The Iowa State University sequencing facility provided DNA sequences using the fluorescent dye-dideoxy terminator method.

Expression and Purification of Wild-type and FBPase Mutants—Protein expression and purification were performed as described previously (16). To avoid contamination of recombinant FBPase by endogenous enzyme, a FBPase-deficient strain of *E. coli* was used in the expression of the enzymes. Protein purity and concentration was confirmed by SDS-polyacrylamide gel electrophoresis (19) and by the Bradford assay (20), respectively. The initial five amino acid residues of the 10DEL and 7DEL mutants were determined by cycles of automated Edman degradation performed by the Iowa State University protein facility.

Circular Dichroism (CD) Spectroscopy—CD spectra of wild-type and mutant FBPases were recorded at room temperature on a Jasco J710 CD spectrometer in a 1-cm cell using a protein concentration of 0.35 mg/ml. Three scans of each spectrum were collected from 200 to 260 nm in increments of 1.3 nm and averaged. Each averaged spectrum was blank-corrected using the software package provided with the instrument.

Kinetic Experiments—Assays for the determination of specific activity, k_{cat}, and activity ratios at pH 7.5/9.5 employed the coupling enzymes phosphoglucose isomerase and glucose-6-phosphate dehydrogenase (1). The reduction of $NADP^+$ to NADPH was monitored spectroscopically at 340 nm. All other assays used the same coupling enzymes but monitored the formation of NADPH by its fluorescence emission at 470 nm using an excitation wavelength of 340 nm. All kinetic assays were performed at room temperature. Initial rates were analyzed using programs written either in the MINITAB language using a α value of 2.0 (21) or by ENZFITTER (22). The kinetic data were fit to several models, and the best fits are reported below.

Steady-state Fluorescence Measurements—Fluorescence data were collected using a SLM 8100C fluorimeter from Spectronic Instruments. The single tryptophan of the Trp-6 mutant was excited selectively using a wavelength of 295 nm. Fluorescence emission spectra were recorded in steps of 1 nm from 310 to 400 nm with a slit width of 2 mm for both excitation and emission and represent the average of five such scans. Fluorescence from AMP-PNP employed excitation and emission wavelengths of 400 and 535 nm, respectively. Conditions under which specific spectra were recorded are provided in the text and figure legends. Each data point for the titration experiments is an average of 15 1-s acquisitions. Enzyme concentrations ranged from 0.3 to 0.5 μM. All spectra were corrected for dilution and inner filter effects (absorbance of light by AMP and AMP-PNP) using the formula (23),

$$F_c = (F - B)(V_i/V_o)10^{(A_{ex}+A_{em})}/2 \quad \text{(Eq. 1)}$$

where F_c is the corrected fluorescence, F is the fluorescence intensity experimentally measured, B is the background, V_i is the volume of the sample for a specific titration point, V_o is the initial volume of the sample, A_{ex} is the absorbance at the wavelength of excitation (295 nm for AMP and 410 for AMP-PNP), and A_{em} is the absorbance at the wavelength of emission (535 nm for AMP-PNP). As a control, ligands caused no change in fluorescence emission after correction from a solution of tryptophan (100 μM) in Hepes buffer (20 mM, pH 7.5).

AMP-PNP titration data were analyzed by nonlinear least squares fits using the following equation.

$$\frac{\Delta F}{F_o} = \frac{(\Delta F_{max}/F_o) \times L^n}{K_d + L^n} \quad \text{(Eq. 2)}$$

where ΔF_{max} is the change in fluorescence caused upon the addition of ligand L, F_o is the fluorescence in the absence of ligand, K_d is the dissociation constant, and n is the Hill coefficient.

RESULTS

Expression, Purification, and Secondary Structure Analysis of Wild-type and Mutant FBPases—Wild-type and mutant FBPases have identical mobilities in chromatographic and electrophoretic separations and are at least 95% pure by SDS-polyacrylamide gel electrophoresis. The pH 7.5/9.5 activity ratios of mutant enzymes (excluding the 7DEL and 10DEL mutants) indicated the absence of proteolyzed enzyme. Results from amino acid sequencing of the 7DEL and 10DEL mutants are consistent with their cDNA, except for the absence of the *N*-formyl methionine. Furthermore, the sequencing data revealed a single N terminus with no background signal indicative of proteolysis. The CD spectra of wild-type and mutant FPBases were essentially superimposable from 200 to 260 nm (data not shown).

Catalytic Rates and Michaelis Constants for Mg^{2+} and $F16P_2$ for Wild-type and Mutant FBPases—Initial rate kinetic studies employed substrate concentrations saturating in $F16P_2$ (20 μM) and Mg^{2+} (10 times K_a-Mg^{2+}) but not so high as to cause inhibition. The deletion mutants have a decreased turnover relative to wild-type FBPase, reducing k_{cat} by 4- and 28-fold for the 7DEL and 10DEL mutants, respectively (Table I). These deletions also caused a 20-fold increase in the K_a for Mg^{2+} and eliminated (10DEL) or reduced (7DEL) Mg^{2+} cooperativity. The 7DEL and 10DEL mutants did not influence the K_m for $F16P_2$. Single point mutations had little affect on k_{cat} relative to the wild-type enzyme; the mutant $Asn^9 \rightarrow$ Ala decreased Mg^{2+} affinity and reduced metal cooperativity. Other point mutations cause only minor changes in kinetic parameters, except for (in some cases) the K_i for AMP.

AMP Inhibition of Wild-type and FBPase Mutants—AMP allosterically inhibits FBPase (5). Complete AMP inhibition of $Ile^{10} \rightarrow$ Asp and 10DEL FBPases requires ~1500-fold more AMP than for the wild-type enzyme. In addition, AMP inhibition is biphasic (Fig. 1). The data presented in Fig. 1, except that for the $Ile^{10} \rightarrow$ Asp and 10DEL FBPases, were fit to Equation 3,

$$v = \frac{V_o}{\left(1 + \left(\frac{I}{IC_{50}}\right)^n\right)} \quad \text{(Eq. 3)}$$

where v is the observed velocity at a specific concentration of AMP, V_o is the fitted velocity in the absence of AMP, I is the concentration of AMP, IC_{50} is the concentration of AMP that causes 50% inhibition, and n is the Hill coefficient. The biphasic curves of the $Ile^{10} \rightarrow$ Asp and 10DEL mutants were fit to Equation 4,

TABLE I
Kinetic parameters for wild-type and mutant forms of fructose-1,6-bisphosphatase

FBPase	pH ratio	k_{cat}	K_m-FBP	K_a-Mg^{2+}	Hill-Mg^{2+}	K_i-$F26P_2$	IC_{50}-AMP	K_i-AMP
		s^{-1}	μM	mM^2		nM	μM	μM^2
Wild type	3.3	22 ± 1	1.8 ± 0.1	0.67 ± 0.04	1.9 ± 0.1	123 ± 5	1.61 ± 0.05	1.19 ± 0.06
10DEL	0.5	0.70 ± 0.04	1.83 ± 0.07	13.2 ± 0.1[a]	0.98 ± .02	45 ± 3	3.2 ± 0.1[b]	0.49 ± 0.03
7DEL	1.3	5.8 ± 0.1	0.72 ± 0.06	11.2 ± 0.7	1.40 ± 0.08	220 ± 10	0.80 ± 0.04	0.42 ± 0.02
D2A	3.7	18.8 ± 0.5	2.03 ± 0.08	1.21 ± 0.05	1.62 ± 0.06	64 ± 3	1.9 ± 0.2	1.5 ± 0.1
F6W	3.3	18.0 ± 0.5	1.58 ± 0.06	0.99 ± 0.05	1.67 ± 0.07	110 ± 10	2.87 ± 0.09	0.78 ± 0.03
D7A	2.6	11.3 ± 0.6	1.8 ± 0.1	1.3 ± 0.1	1.56 ± 0.09	60 ± 4	0.70 ± 0.01	0.62 ± 0.03
T8A	4.6	25 ± 2	2.1 ± 0.1	1.4 ± 0.1	1.7 ± 0.1	173 ± 8	0.87 ± 0.03	0.36 ± 0.03
N9A	3.3	21.2 ± 0.9	0.63 ± 0.03	6.6 ± 0.3	1.50 ± 0.06	76 ± 1	1.08 ± 0.03	0.59 ± 0.04
I10M	3.1	15.3 ± 0.6	2.0 ± 0.1	1.28 ± 0.04	1.71 ± 0.04	76 ± 7	2.85 ± 0.06	0.57 ± 0.05
I10D	3.0	16.7 ± 0.4	1.2 ± 0.1	0.56 ± 0.05	2.0 ± 0.1	81 ± 8	2.75 ± 0.09[b]	2.7 ± 0.2

[a] K_a for 10DEL is reported in mM.
[b] Data reported are for the high affinity site, IC_{50} for low affinity sites >20 mM.

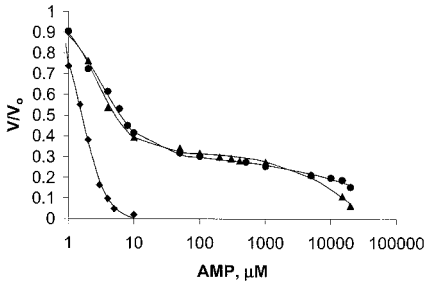

FIG. 1. **AMP inhibition of wild-type and mutant FBPases.** AMP titrations are of wild-type (♦), $Ile^{10} \rightarrow Asp$ (●), and 10DEL (▲) FBPases in saturating $F16P_2$ (20 μM) and a Mg^{2+} concentration equal to the K_a for Mg^{2+} of each enzyme. See text for details regarding the fitted curves.

$$v = \frac{V_o}{\left(1 + \left(\frac{I}{IC_{50\text{-high}}}\right)^2 + \left(\frac{I}{IC_{50\text{-low}}}\right)^n\right)} \qquad \text{(Eq. 4)}$$

where v, V_o, and I are as above in Equation 3, and $IC_{50\text{-high}}$ and $IC_{50\text{-low}}$ represent concentrations of AMP that cause 50% relative inhibition due to the ligation of high and low affinity sites, respectively. Ligation of the high affinity sites, as shown below, is cooperative with a Hill coefficient of 2, whereas the cooperativity with respect to the ligation of the low affinity sites is an adjustable parameter (n) in Equation 4. The fitted value for n is 0.68 ± 0.09 and 0.39 ± 0.05 for the $Ile^{10} \rightarrow Asp$ and 10DEL enzymes, respectively. The positive cooperativity for the high affinity interaction of AMP (the exponent for the $I/IC_{50\text{-high}}$ term is 2) is justified by the analysis of kinetics data depicted in Fig. 2 using low concentrations of AMP (0–10 μM). These (as well as data for FBPases that do not exhibit biphasic inhibition by AMP) fit very well to Equation 5 (goodness of fit between 2.6 and 5.3%),

$$\frac{1}{v} = \frac{1}{V_m}\left(1 + \frac{K_a}{A^n}\left(1 + \frac{I^n}{K_i}\right)\right) \qquad \text{(Eq. 5)}$$

where v, V_m, A, I, K_a, K_i, and n represent, respectively, initial velocity, maximal velocity, Mg^{2+} concentration, AMP concentration, the Michaelis constant for Mg^{2+}, the dissociation constant for AMP from the enzyme-AMP complex, and the Hill coefficient for AMP. All mutants (except 10DEL) exhibited both Mg^{2+} and AMP cooperativity ($n = 2$). The 10DEL mutant retained AMP cooperativity ($n = 2$), but Mg^{2+} cooperativity was eliminated ($n = 1$).

$F26P_2$ Inhibition of Wild-type and Mutant FBPases—$F26P_2$ is a substrate analog that binds at the active site of the enzyme. The K_i values for $F26P_2$ listed in Table I were determined by fitting the data (not shown) to Equation 2, a model for linear competitive inhibition (goodness of fit between 2.1 and 3.6%),

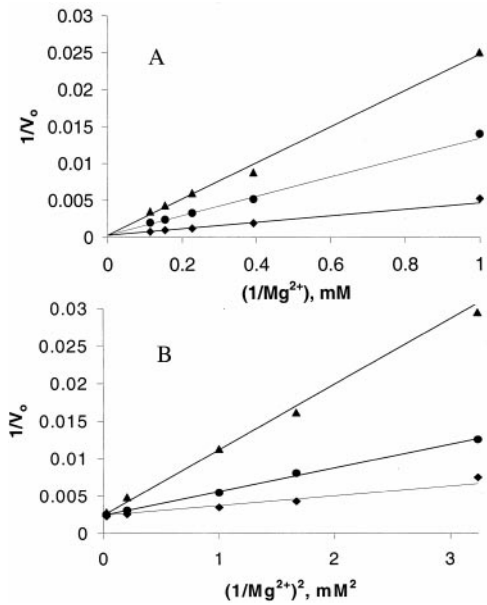

FIG. 2. **Kinetic mechanism of AMP inhibition of $Ile^{10} \rightarrow Asp$ and 10DEL FBPases.** AMP competes with Mg^{2+} in both the 10DEL (*A*) and $Ile^{10} \rightarrow Asp$ (*B*) mutants. Concentrations of AMP are 0 (♦), 1 (●), and 1.5 μM (▲) (*A*) and 0 (♦), 2 (●), and 4 μM (▲) (*B*).

$$\frac{1}{v} = \frac{1}{V_M}\left(1 + \frac{K_b}{B}\left(1 + \frac{I}{K_i}\right)\right) \qquad \text{(Eq. 6)}$$

where v and V_M are as above, I is the concentration of $F26P_2$, B is the concentration of $F16P_2$, K_b is the Michaelis constant for $F16P_2$, and K_a is the dissociation constant for $F26P_2$ from the $F26P_2$-enzyme complex. The mechanism of $F26P_2$ inhibition is the same for all mutant and the wild-type FBPases.

Fluorescence Emission from $Phe^6 \rightarrow Trp$ and AMP-PNP—As wild-type FBPase has no tryptophan residues, the substitution of tryptophan for phenylalanine at position 6 introduces a unique spectroscopic probe. The kinetic properties of $Phe^6 \rightarrow Trp$ FBPase are nearly identical to those of the wild-type enzyme (Table I). Furthermore, the fluorescence emission spectrum of the $Phe^6 \rightarrow Trp$ mutant changes by only 7% in its emission maximum in the presence and absence of saturating AMP, with no observable change in the wavelength of maximum emission.

The fluorescent AMP analogue, AMP-PNP, and AMP inhibit wild-type FBPase by identical kinetic mechanisms, with nearly identical kinetic parameters (16). AMP-PNP has the advantage compared with AMP of exhibiting a significant increase in fluorescence emission upon its binding to the allosteric pocket of FBPase. Hence, for mutants of FBPase that exhibit a significant loss in AMP inhibition due to mutation, one can use

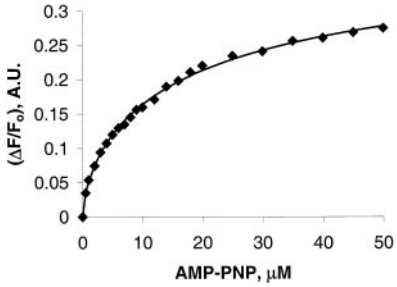

FIG. 3. **AMP-PNP titration of the 10DEL mutant.** Fluorescence of AMP-PNP observed in the presence of 0.5 μM 10DEL. A wavelength of 400 nm was used for excitation, and fluorescence emission was monitored at 535 nm. *A.U.*, arbitrary units.

AMP-PNP to distinguish whether the change is due to impaired binding or to an impaired mechanism of allosteric inhibition. In the cases of the 10DEL (Fig. 3) and $Ile^{10} \rightarrow Asp$ (data not shown) FBPases, dissociation constants for AMP-PNP are comparable with that determined for the wild-type enzyme (16).

DISCUSSION

Crystal structures of FBPase from mammalian sources and the chloroplast have little or no electron density for the N-terminal region of the enzyme. Yet certain amino acids in this region, particularly residues 9–10, are conserved over a wide range of organisms. As porcine FBPase has no tryptophan, incorporation of a tryptophan for Phe^6 introduces a unique spectroscopic probe. The functional properties of $Phe^6 \rightarrow Trp$ FBPase are comparable with those of the wild-type enzyme, and fluorescence emission in the presence and absence of AMP is about the same. Evidently, the first six residues of porcine FBPase have no functional role in catalysis or metabolite regulation of catalysis.

Position 7 may be the first residue from the N terminus to directly or indirectly influence the functional properties of FBPase. Asp^7 is the first residue defined by electron density in crystal structures of wild-type FBPase (14). The 7DEL construct exhibits significant changes in functional properties (Table I), in particular K_a-Mg^{2+} is elevated 15-fold relative to that of wild-type FBPase. $Asp^7 \rightarrow Ala$ FBPase, however, has functional properties similar to those of the wild-type enzyme. Hence, the functional changes due to the 7DEL construct may be the consequence of an indirect perturbation on the conformation of residues 9–10 and/or the conformational properties of loop 52–72 in the R-state (AMP absent). Interestingly, the mutation of the Lys^{50} to proline (a hinge element for loop 52–72) eliminates AMP inhibition by the disruption of the allosteric mechanism and also causes a 15-fold elevation in K_a-Mg^{2+} (16). Other mutations in the segment 50–55 cause little effect on AMP inhibition but increase K_a-Mg^{2+} by 10-fold or more.[2]

The impact of the 10DEL construct on the functional properties of FBPase is even more extreme than is that of the 7DEL mutant. The low pH activity ratio is consistent with the effects of the mutation of Lys^{50} to Pro (16) and of the truncation of 25 residues from the N terminus by proteolysis of FBPase (24). The low pH-activity ratio could result from the proteolysis of loop 52–72 (25); however, N-terminal sequencing of the 10DEL mutant excludes this possibility. Instead, the 15-fold increase in K_a-Mg^{2+} and the 30-fold decrease in k_{cat} is consistent with the failure of loop 52–72 to achieve an engaged conformation in the R-state of the 10DEL construct. The effects of the 10DEL mutant can be explained in part by the side chain at position 9. $Asn^9 \rightarrow Ala$ FBPase exhibits a 10-fold increase in its K_a-Mg^{2+}

[2] C. Iancu, H. J. Fromm, and R. B. Honzatko, unpublished data.

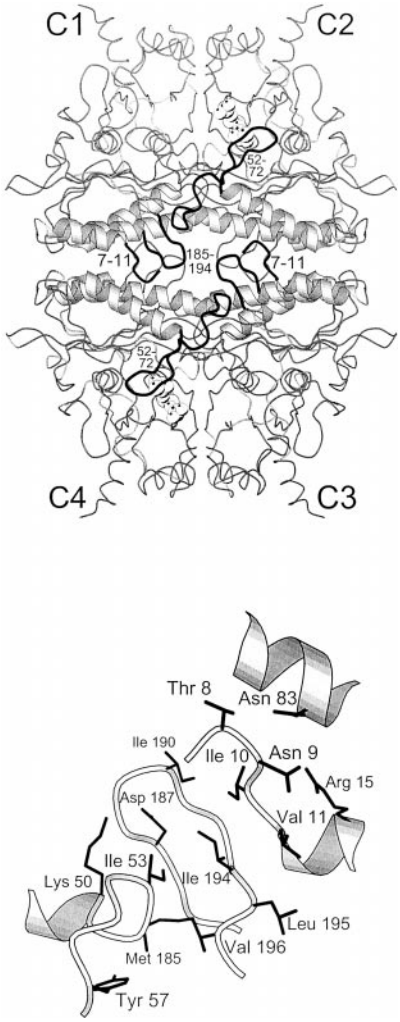

FIG. 4. **Structural elements important to allosteric regulation in the R-state of FBPase.** The tetramer as viewed down one of its three, mutually perpendicular symmetry axes in the R-state (*top*). Loop 52–72 is in the engaged conformation. Residues near the hinge of this loop in subunit C4 pack against loop 182–194 of subunit C3, which in turn pack against residues 7–11 of the N-terminal segment preceding helix H1 of subunit C3 (*bottom*). Residues 7–11 lie in a groove bordered by helix H3 of subunit C2 and loop 182–194 of subunit C3. Orientations of top and bottom illustrations are the same. This illustration was drawn with MOLSCRIPT (33).

but no change in k_{cat} or the pH-activity ratio relative to the wild-type enzyme. In R-state crystal structures, Asn^9 hydrogen bonds with Arg^{15} (Fig. 4). The Asn^9-Arg^{15} interaction probably stabilizes residues 7–11 in their R-state conformation. These residues pack between helix 3 and loop 187–194. Loop 187–194 interacts through hydrogen bonds and nonbonded contacts with hinge residues preceding loop 52–72 (Fig. 4). The loss of the Asn^9-Arg^{15} hydrogen bond may lead to a long range conformational change, which destabilizes the engaged conformation of loop 52–72. Indeed, the disordered conformation of loop 52–72 appears hand in hand with disorder in residues 1–11 in R-state crystal structures (9, 18).

Unlike the 7DEL construct, which has little effect on allosteric inhibition by AMP, the 10DEL mutation significantly alters the maximum level of AMP inhibition. The 25-residue truncated form of FBPase is not inhibited by AMP (24). As some of the 25 residues are part of the AMP binding pocket (14), the effect of limited proteolysis is of little surprise. In contrast, the first 10 residues are remote from the site of AMP binding, and indeed, AMP-PNP binds with nearly identical affinity constants to 10DEL and wild-type FBPases. Changes

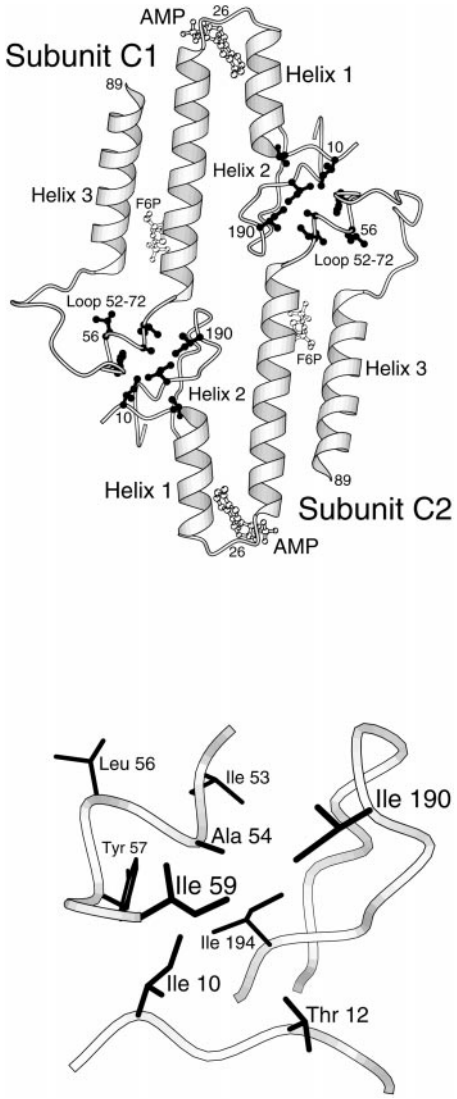

FIG. 5. **Structural elements important to allosteric regulation in the T-state of FBPase.** Shown here are segments of two polypeptide chains (residues 9–89) viewed down an axis of molecular 2-fold symmetry toward the interface buried between subunits C1-C2 and subunits C3-C4 (*top*). The side chain of Ile^{10} from subunit C2 makes nonbonded contacts with Thr^{12} and Ile^{194}, both from subunit C2, and Tyr^{57} and Ile^{59}, both from loop 52–72 of subunit C1 (*bottom*). Orientations of top and bottom illustrations are the same. This illustration was drawn with MOLSCRIPT (33).

in the functional properties due to the 10DEL mutant, then, must result from perturbations in the allosteric mechanism of AMP inhibition. Although no single point mutation reproduced the functional properties of the 10DEL construct in the absence of AMP, the mutation of Ile^{10} to aspartate reproduced the phenomenon of 50% maximal inhibition by AMP. As noted below, the hydrophobic side chain at position 10 is critical to the stability of the disengaged conformation of loop 52–72 in the T-state.

The following model is a basis for understanding AMP inhibition in wild-type FBPase and in mutant FBPases. Hereafter, T-state and R-state refer to quaternary arrangements of subunits in FBPase, distinguished by the 17° rotation about a molecular symmetry axis. In addition, the subunits in the T- and R-states can adopt different tertiary conformations, the most significant of which involve conformational changes in loop 52–72. In the T-state of wild-type FBPase, loop 52–72 is in the disengaged conformation. The T-state subunit arrangement stabilizes the disengaged conformation by interactions, which involve residues 50–60 of subunit C1 with residues 187–194 and 9–11 of subunit C2 (Fig. 5). Point mutations in these structural elements profoundly influence AMP inhibition (16, 26, 27), AMP cooperativity (26, 27), $F26P_2$ inhibition (16, 27), and/or metal affinity (16). The R-state subunit arrangement does not stabilize the disengaged loop conformation. As a consequence loop 52–72 occupies an engaged conformation or a disordered conformation. The engaged conformation was first observed in the context of a product-Zn^{2+} complex of the wild-type enzyme (13). The disordered conformation of loop 52–72 appears in FBPase structures crystallized in the absence of metal activators (18).

Catalysis occurs at neutral pH if loop 52–72 can cycle between its engaged and disordered conformations. A loop that is always engaged is a dead-end complex. A loop that cannot achieve the engaged conformation results in low metal affinity and little or no activity at neutral pH. Assuming loop 52–72 exchanges between its engaged and disordered conformations, the free energy differences between these conformational states must be small, that is, the R-state maintains small free-energy differences between disordered and engaged conformations of loop 52–72. In contrast, the T-state subunit arrangement selectively stabilizes a new conformation for loop 52–72 (disengaged conformation), which de-populates the disordered/engaged loop conformations. The decline in the catalytic rate of T-state FBPase is directly related to the differences in free energy between the engaged/disordered loop conformations and the disengaged loop conformation. For the wild-type enzyme, the free energy difference is large; hence, little or no catalysis occurs. For specific mutants of FBPase that selectively destabilize the disengaged loop conformation, the free energy difference is less, the engaged/disordered loop conformations are more populated, and hence, a measurable level of catalysis occurs. Biphasic AMP inhibition should appear whenever a mutation selectively destabilizes the disengaged loop conformation of the T-state. FBPase mutants with biphasic AMP inhibition ($Lys^{42} \rightarrow Ala$, $Glu^{192} \rightarrow Ala$, $Glu^{192} \rightarrow Gln$, $Lys^{50} \rightarrow Asn$, $Lys^{50} \rightarrow Pro/Tyr^{57} \rightarrow Trp$, and $Ile^{10} \rightarrow Asp$) exhibit plateau activities, which vary from 10 to 70% full activity (16, 26, 27). As suggested by Kantrowitz and co-workers (28), the activity most likely comes from FBPase in the T-state subunit arrangement. Here we add that some fraction of the mutant FBPases have engaged/disordered loop conformations in the presence of AMP, which are responsible for the observed turnover. The free energy relationships of the model are summarized in Fig. 6.

From the model above, mutant FBPases with biphasic AMP inhibition must have a less stable, disengaged conformation of loop 52–72 in the T-state. In fact, structural evidence supports this claim. The disengaged loop in the T-state of wild-type FBPase has interpretable electron density up to residue 60, with the residues 50–60 participating in interactions across the C1-C2 subunit interface (14). The mutation of Lys^{42} to alanine results in biphasic AMP inhibition with 70% relative activity at the plateau (26). The crystal structure of the AMP complex of the $Lys^{42} \rightarrow Ala$ mutant is in the T-state, but loop 52–72 is poorly ordered from residues 54 to 72 (28). In the crystal structure of the AMP complex of $Ile^{10} \rightarrow Asp^2$ the enzyme is again in the T-state, and loop 52–72 is without electron density from residues 54 to 72. Hence, loop 52–72 in the Ala^{42} and Asp^{10} mutants is not in the disengaged conformation of wild-type FBPase but, rather, in a disordered conformation similar to that of the R-state apoenzyme. If the disengaged structure is de-populated in favor of disordered conformations, then perhaps under the appropriate conditions an engaged conformation for loop 52–72 may occur in the

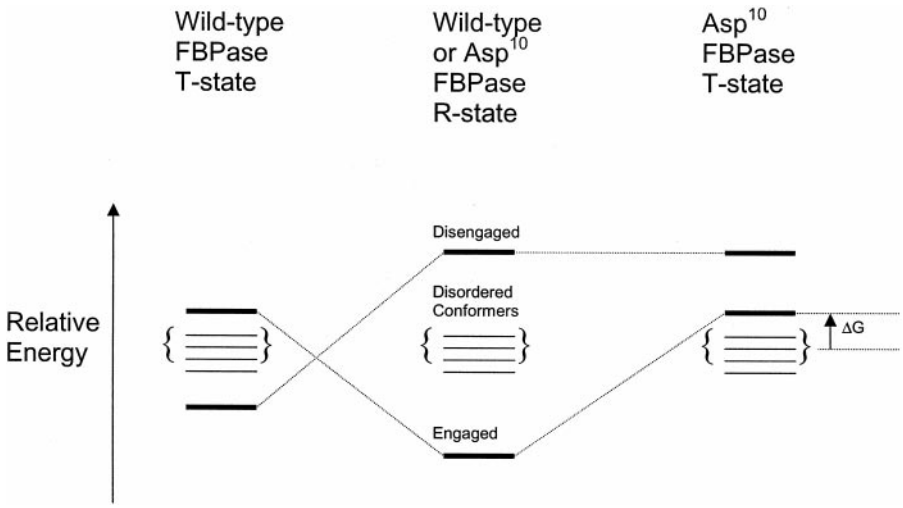

FIG. 6. **Changes in relative free energy levels of three loop conformations in the R- and T-states of wild-type and Asp^{10} FBPases.** *Bold lines* indicate the energies of the engaged and disengaged conformations of loop 52–72, whereas the bundle of *fine lines* represents the disordered loop, which is in a manifold of conformational states with nearly equivalent free energies. In the wild-type enzyme, the R to T transition selectively stabilizes the disengaged conformation of loop 52–72 over the engaged and disordered conformational states. In the Ile^{10} → Asp mutant, the T-state does not stabilize a disengaged conformation for loop 52–72. The separation in free energy between the engaged conformation and the disordered conformation in the T-state (ΔG in figure) may influence the observed level of catalytic activity in the presence of saturating AMP.

T-state of such mutants.

The thioredoxin-mediated formation of a disulfide bond between Cys^{153} and Cys^{173} in chloroplast FBPase (29) putatively stabilizes the position of a loop that excludes the binding of metal activators and the engaged conformation of loop 61–81 (which corresponds to loop 52–72 of mammalian FBPase) (30). FBPase from the chloroplast evidently does not bind AMP (30, 31). Yet existing crystal structures of reduced and oxidized chloroplast FBPase have nearly the same quaternary arrangement of subunits, resembling most closely the T-state of mammalian FBPase. Hence, as illustrated by FBPase from the chloroplast, a T-state subunit arrangement by itself does not exclude catalysis. Interestingly, position 18 of the chloroplast enzyme, which corresponds to position 10 of mammalian FBPase, is isoleucine, this residue being widely conserved among FBPases. Furthermore, in the inactive, oxidized form of chloroplast FBPase, loop 61–81 (corresponding to loop 52–72 of the mammalian enzyme) is in the disengaged conformation (30), whereas the equivalent loop in the active, reduced form of chloroplast FBPase is in the disordered conformation (32). Evidently, oxidation and reduction of the disulfide bond in chloroplast FBPase influences the relative stability of the disengaged loop-conformation in a manner similar to that of AMP in mammalian FBPases. The observation of corresponding conformational states in mammalian and chloroplast FBPases infers a common, early mechanism of FBPase regulation that has diverged through evolution.

REFERENCES

1. Benkovic, S. T., and de Maine, M. M. (1982) *Adv. Enzymol. Relat. Areas Mol. Biol.* **53,** 45–82
2. Tejwani, G. A. (1983) *Adv. Enzymol. Relat. Areas Mol. Biol.* **54,** 121–194
3. Van Schaftingen, E. (1987) *Adv. Enzymol. Relat. Areas Mol Biol.* **59,** 45–82
4. Pilkis, S. J., el-Maghrabi, M. R., and Claus T. H. (1988) *Annu. Rev. Biochem.* **57,** 755–783
5. Nimmo, H. G., and Tipton, K. F. (1975) *Eur. J. Biochem.* **58,** 567–574
6. Liu, F., and Fromm, H. J. (1988) *J. Biol. Chem.* **263,** 9122–9128
7. Scheffler, J. E., and Fromm, H. J. (1986) *Biochemistry* **25,** 6659–6665
8. Xue, Y., Huang, S., Liang, J. Y., Zhang, Y., and Lipscomb W. N. (1994) *Proc. Natl. Acad. Sci. U. S. A.* **99,** 12482–12486
9. Zhang, Y. Liang, J.-Y., Huang, S., and Lipscomb, W. N. (1994) *J. Mol. Biol.* **244,** 609–624
10. Shyur, L. -F., Aleshin, A. E., Honzatko, R. B., and Fromm, H. J. (1996) *J. Biol. Chem.* **271,** 33301–33307
11. Ke, H. M., Zhang, Y. P., and Lipscomb, W. N. (1990) *Proc. Natl. Acad. Sci. U. S. A.* **87,** 5243–5247
12. Villeret, V., Huang, S., Zhang, Y., and Lipscomb, W. N. (1995) *Biochemistry* **34,** 4307–4315
13. Choe, J. -Y., Poland B. W., Fromm, H. J., and Honzatko, R. B. (1998) *Biochemistry* **33,** 11441–11450
14. Choe, J. Y., Fromm, H. J., and Honzatko, R. B. (2000) *Biochemistry* **39,** 8565–8574
15. Kurbanov, F. T., Choe, J. -Y., Honzatko, R. B., and Fromm, H. J. (1998) *J. Biol. Chem.* **273,** 17511–17516
16. Nelson, S. W., Choe, J. -Y., Honzatko, R. B., and Fromm, H. J. (2000) *J. Biol. Chem.* **275,** 29986–29992
17. Nelson, S. W., Choe, J.-Y., Iancu, C. V., Honzatko, R. B., and Fromm, H. J. (2000) *Biochemistry* **39,** 11100–11106
18. Ke, H., Thorpe, C. M., Seaton, B. A., Marcus, F., and Lipscomb, W. N. (1989) *Proc. Natl. Acad. Sci. U. S. A.* **86,** 1475–1479
19. Laemmli, U. K. (1970) *Nature* **227,** 680–685
20. Bradford, M. M. (1976) *Anal. Biochem.* **72,** 248–252
21. Lui, F., and Fromm, H. J. (1990) *J. Biol. Chem.* **265,** 7401–7406
22. Leatherbarrow, R. J. (1987) *ENZFITTER: A Non-Linear Regression Data Analysis Program for the IBM PC*, pp. 13–75, Elsevier Science Publishers B. V., Amsterdam
23. Lakowicz, J. R. (1999) *Principles of Fluorescence Spectroscopy*, 2nd Ed., pp. 52–54, Kluwer Academic Publishers/Plenum Publishers, New York
24. Chatterjee, T., Reardon, I., Heinrikson, R. L., and Marcus, F. J. (1985) *J. Biol. Chem.* **260,** 13553–13359
25. Horecker, B. L., Melloni, E., and Pontremoli, S. (1975) *Adv. Enzymol. Relat. Areas Mol. Biol.* **42,** 193–226
26. Lu, G., Giroux, E. L., and Kantrowitz, E. R. (1997) *J. Biol. Chem.* **272,** 5076–5081
27. Carcamo, J. G., Yanez, A. J., Ludwig, H. C., Leon, O., Pinto, R. O., Reyes, A. M., and Slebe, J. C. (2000) *Eur. J. Biochem.* **267,** 2242–2251
28. Lu, G., Stec, B., Giroux, E. L., and Kantrowitz, E. R. (1996) *Protein Sci.* **5,** 2333–2342
29. Jacquot, J. P., Lopez-Jaramillo, J., Miginiac-Maslow, M., Lemaire, S., Cherfils, J., Chueca, A., and Lopez-Gorge, J. (1997) *FEBS Lett.* **401,** 143–147
30. Chiadmi, M., Navaza, A., Miginiac-Maslow, M., Jacquot, J. P., and Cherfils, J. (1999) *EMBO J.* **18,** 6809–6815
31. Nel, W., and Terblanche, S. E. (1992) *Int. J. Biochem.* **24,** 1267–1283
32. Villeret, V., Huang, S., Zhang, Y., Xue, Y., and Lipscomb, W. N. (1995) *Biochemistry* **34,** 4299–4306
33. Kraulis, J. (1991) *J. Appl. Crystallogr.* **24,** 946–950

The N-terminal Segment of Recombinant Porcine Fructose-1,6-bisphosphatase Participates in the Allosteric Regulation of Catalysis

Scott W. Nelson, Feruz T. Kurbanov, Richard B. Honzatko and Herbert J. Fromm

J. Biol. Chem. 2001, 276:6119-6124.
doi: 10.1074/jbc.M009485200 originally published online November 28, 2000
